

# Nonlinear Evolution and Final Fate of Charged Anti-de Sitter Black Hole Superradiant Instability

Pablo Bosch,<sup>1, 2, \*</sup> Stephen R. Green,<sup>2, †</sup> and Luis Lehner<sup>2, ‡</sup>

<sup>1</sup>*Department of Physics & Astronomy and Guelph-Waterloo Physics Institute  
University of Waterloo, Waterloo, Ontario N2L 3G1, Canada*

<sup>2</sup>*Perimeter Institute for Theoretical Physics, Waterloo, Ontario N2L 2Y5, Canada*

We describe the full nonlinear development of the superradiant instability for a charged massless scalar field, coupled to general relativity and electromagnetism, in the vicinity of a Reissner-Nordström-AdS black hole. The presence of the negative cosmological constant provides a natural context for considering perfectly reflecting boundary conditions and studying the dynamics as the scalar field interacts repeatedly with the black hole. At early times, small superradiant perturbations grow as expected from linearized studies. Backreaction then causes the black hole to lose charge and mass until the perturbation becomes nonsuperradiant, with the final state described by a stable hairy black hole. For large gauge coupling, the instability extracts a large amount of charge per unit mass, resulting in greater entropy increase. We discuss the implications of the observed behavior for the general problem of superradiance in black hole spacetimes.

**Introduction.**—A bosonic field can extract energy from a rotating black hole (BH) through superradiant scattering [1, 2], resulting in an increase in field amplitude. If, in addition, the field is reflected by a potential barrier sufficiently far away, then this amplification process repeats, resulting in exponential growth. This is known as the superradiant instability or “black hole bomb” [3]. Since in global anti-de Sitter (AdS) spacetime, naturally reflecting boundary conditions at  $\mathcal{I}$  can be defined, asymptotically AdS black holes with ergoregions are subject to the superradiant instability [4–6].

A similar process occurs for Reissner-Nordström (RN) BHs [4, 7–9], with the charge playing the role of the angular momentum. There, a charged scalar field mode with time dependence  $\psi \sim e^{-i\omega t}$  is superradiantly amplified if  $\omega r_H < qQ$  ( $r_H$  is the BH outer horizon radius,  $Q$  is the BH charge, and  $q$  is the gauge coupling of the scalar field). In the RN-AdS case [4, 10], the reflecting boundary implies that there is a minimum mode frequency, so the instability sets in when  $Qq > \frac{3r_H}{L}$ , where  $L$  is the AdS scale (in the limit of small  $r_H/L$ ).

When perturbations are small, the description above is valid and a linearized analysis is suitable; several studies have determined the quasinormal mode spectra of, e.g., Kerr-AdS [5, 11] and RN-AdS [10]. As the perturbation grows, however, the backreaction on the spacetime becomes significant, and this description breaks down.

Less is known about the final state of the instability, although it is, in general, expected to be a “hairy” BH. In the RN-AdS case, static BHs surrounded by a scalar field condensate have been constructed, and have been conjectured to be the end point of the instability [12, 13]. In the Kerr-AdS case, rotating BHs with a single helical Killing vector field have been constructed [14], but these BHs are unstable themselves and are, therefore, not plausible end points. The final state might be a hairy BH without any symmetries, or the instability may lead to a violation of cosmic censorship [15]. Further complication

arises from the fact that gravitational interactions can result in significant nonlinear mode coupling in confined geometries such as AdS, where dissipation is low [16, 17].

It is of wide interest to have a more complete picture of the dynamics and end point of the superradiant instability. In astrophysics, the instability is used to constrain dark matter models and may lead to observable gravitational wave emissions [18–20]. In holography (AdS/CFT [21] and Kerr/CFT [22]) superradiance manifests within the CFT [11, 23–26], and the nonlinear evolution plays a role in determining the final thermal state. Finally, questions of BH instabilities are of theoretical interest in classical general relativity [6, 27, 28].

Fully analyzing the superradiant instability is complicated by several factors: large differences in scale between the BH and perturbation, long instability time scales, fully nonlinear equations (Einstein and other fields), and an intrinsically  $(3+1)$ -dimensional problem. Thus, nonlinear simulations, while the obvious approach, are challenging [29, 30]; however, see [31]. In the charged case, however, the instability is present even in spherical symmetry, and the instability time scale is shorter. By studying this case, one could hope to draw general conclusions that could be applied more broadly.

In this Letter we study the nonlinear evolution of the superradiant instability of RN-AdS BHs in spherical symmetry. We verify the initial growth rates predicted from the linear theory, and we confirm expectations that the final state is a hairy BH<sup>1</sup>. At intermediate times, we track the dynamics of individual modes as charge and mass are nonlinearly extracted from the BH, and we arrive at an

<sup>1</sup> These results are consistent with very recent results of [32] for the case of RN surrounded by an artificial mirror (which appeared while we were completing our work). Working in AdS provides a natural setting free of ambiguities and potential sources of constraint violations.

intuitive picture of the behavior. In particular, within this picture, the behavior characterized as a “bosonova” of [32] for large values of  $q$  can be easily understood.

**Model.**—We follow the conventions of [33], and we work in  $d = 4$  dimensions. The Lagrangian density is

$$16\pi G_N \mathcal{L} = R + \frac{6}{L^2} - \frac{1}{4} F_{ab} F^{ab} - |D_a \psi|^2, \quad (1)$$

where  $D_a \equiv \nabla_a - iqA_a$  is the gauge covariant derivative. This gives rise to the Einstein equation

$$G_{ab} - \frac{3}{L^2} g_{ab} = 8\pi T_{ab}^\psi + 8\pi T_{ab}^{\text{EM}}, \quad (2)$$

where the stress-energy tensors are

$$8\pi T_{ab}^{\text{EM}} = \frac{1}{2} \left( g^{cd} F_{ac} F_{bd} - \frac{1}{4} g_{ab} F_{cd} F^{cd} \right), \quad (3)$$

$$8\pi T_{ab}^\psi = \frac{1}{2} [(D_a \psi)^* (D_b \psi) + \text{c.c.}] - \frac{1}{2} g_{ab} |D_c \psi|^2. \quad (4)$$

The Maxwell and scalar field equations are

$$\nabla^b (\nabla_b A_a - \nabla_a A_b) = iq\psi^* D_a \psi - iq\psi (D_a \psi)^*, \quad (5)$$

$$D^a D_a \psi = 0. \quad (6)$$

The RN-AdS BH solves the field equations, with metric  $ds^2 = -f dt^2 + f^{-1} dr^2 + r^2 d\Omega_2^2$ , where  $f = 1 - \frac{2M}{r} + \frac{Q^2}{4r^2} + \frac{r^2}{L^2}$ ; Maxwell field  $A_\mu dx^\mu = \left( \frac{Q}{r} - \frac{Q}{r_H} \right) dt$ ; and  $\psi = 0$ . The  $-\frac{Q}{r_H}$  term in the Maxwell field is a gauge choice to have the field vanish at the horizon.

**Numerical Method.**—Our simulations follow the general approach of [34]. We adopt ingoing Eddington-Finkelstein coordinates and spherical symmetry<sup>2</sup> so that the metric takes the form

$$ds^2 = -A(v, r) dv^2 + 2dv dr + \Sigma(v, r)^2 d\Omega_2^2. \quad (7)$$

For the Maxwell field, we work in a gauge where

$$A_\mu dx^\mu = W(v, r) dv, \quad (8)$$

and we require  $\psi = \psi(v, r)$ . With these choices, the

equations of motion (2), (5), and (6) take the form

Einstein:

$$0 = \Sigma (d_+ \Sigma)' + (d_+ \Sigma) \Sigma' - \frac{3}{2L^2} \Sigma^2 - \frac{1}{2} + \frac{1}{8} \Sigma^2 W', \quad (9)$$

$$0 = A'' - \frac{4}{\Sigma^2} (d_+ \Sigma) \Sigma' + \frac{2}{\Sigma^2} + (\psi')^* d_+ \psi + (d_+ \psi)^* \psi' - (W')^2 + iqW [\psi^* \psi' - (\psi')^* \psi], \quad (10)$$

$$0 = d_+ d_+ \Sigma - \frac{1}{2} A' d_+ \Sigma + \frac{1}{2} \Sigma |d_+ \psi|^2 + \frac{1}{2} q^2 W^2 \Sigma |\psi|^2 + \frac{1}{2} iqW \Sigma [\psi^* d_+ \psi - \psi (d_+ \psi)^*], \quad (11)$$

$$0 = \Sigma'' + \frac{1}{2} \Sigma |\psi'|^2, \quad (12)$$

Maxwell:

$$0 = (d_+ W)' - \frac{1}{2} A' W' + 2 \frac{d_+ \Sigma}{\Sigma} W' - 2q^2 W |\psi|^2 + iq [\psi^* d_+ \psi - \psi (d_+ \psi)^*], \quad (13)$$

$$0 = W'' + \frac{2}{\Sigma} \Sigma' W' + iq [\psi^* \psi' - \psi (\psi')^*], \quad (14)$$

Scalar:

$$0 = 2(d_+ \psi)' + 2 \frac{\Sigma'}{\Sigma} d_+ \psi + 2 \frac{d_+ \Sigma}{\Sigma} \psi' - iq\psi W' - 2iq \frac{\Sigma'}{\Sigma} W \psi - 2iqW \psi', \quad (15)$$

where we denote  $f' \equiv \partial_r f$ , and the derivative along the outgoing null direction,  $d_+ f \equiv \partial_v f + \frac{1}{2} A \partial_r f$ .

The equations of motion are solved imposing reflecting boundary conditions at  $r \rightarrow \infty$ . These take the form

$$A = \frac{r^2}{L^2} + \lambda r + \left( 1 + \frac{L^2 \lambda^2}{4} - L^2 \dot{\lambda} \right) - \frac{2M}{r} + \left( L^2 \lambda M + \frac{Q^2}{4} \right) \frac{1}{r^2} + O(r^{-3}), \quad (16)$$

$$\Sigma = r + L^2 \lambda / 2 + O(r^{-5}), \quad (17)$$

$$W = \nu + Q/r + O(r^{-2}), \quad (18)$$

$$\psi = \varphi_3/r^3 + O(r^{-4}). \quad (19)$$

The constants  $M$  and  $Q$  represent the ADM mass and charge, respectively; these are prescribed as boundary data. The functions  $\lambda(v)$  and  $\nu(v)$  represent the remaining gauge freedom after putting the metric and Maxwell fields into the forms (7)–(8). We make the further gauge choice that  $\lambda = \nu = 0$ . Finally the function  $\varphi_3(v)$  is an unknown function that is determined by the solution.

The procedure to integrate the equations is as follows: On an initial time slice  $v = v_0$  we prescribe the function  $\psi(v_0, r)$ . We then integrate, radially inwards in  $r$  [and subject to the asymptotic conditions (16)–(19)], eqs. (9), (10), (12), (14), and (15), to obtain  $d_+ \Sigma$ ,  $A$ ,  $\Sigma$ ,  $W$ , and  $d_+ \psi$ , respectively, at time  $v = v_0$ . From  $d_+ \psi$ ,  $\psi$ , and  $A$ , we obtain  $\partial_v \psi$  at time  $v = v_0$ . By integrating in time, we obtain  $\psi$  at the next time step. The procedure may then be iterated. Equations (11) and (13) are redundant, and we use these as independent residuals to test our code.

<sup>2</sup> This differs from the analysis of [35], which imposed planar symmetry and studied the nonlinear evolution of a holographic superconductor.

We use finite differences, using a mixed second and fourth order radial and fourth order in time Runge-Kutta method. The spatial domain extends from an inner radius  $r_0$ —several grid points within the BH—to infinity. In fact, we compactify this domain by introducing a new spatial coordinate  $\rho = 1/r$ . This gives rise to a compact domain  $0 \leq \rho \leq 1/r_0$ , which we discretize in a uniform grid.

For initial data, we take the scalar field to be compactly supported, with  $\psi = (r^{-1} - r_1^{-1})^3(r^{-1} - r_2^{-1})^3/r^2[\kappa_1 + \kappa_2 \sin(10/r)]$  if  $r \in [r_1, r_2]$  (and zero otherwise). For production runs we typically use  $\{\kappa_1, \kappa_2\} = 10^{-4}$ , so the scalar field is initially negligible compared to the BH, and  $\{r_1, r_2\} = \{2M, 3M\}$ . We checked by varying  $\{\kappa_1, \kappa_2\}$  that different initial data do not affect the features of the final solution, provided the amplitude is small. We set  $L = 1$ ,  $M = 0.1$  and  $Q = -0.18115$ ; this corresponds to a BH small compared to the AdS scale ( $r_H = 0.138$ ), with charge 63.9% of the critical value. Excellent accuracy is obtained with grid sizes of  $N = 1600n + 1$  points (with  $n = 1$  for low  $q$  and  $n = 2, 3$  for higher ones), and we have thoroughly tested our implementation (see the Supplemental Material).

**Results.**—Having fixed  $M$  and  $Q$ , we varied the gauge coupling  $q$  of the scalar field. At early times, simulations reveal that for sufficiently small  $q \lesssim \frac{3r_H}{QL}$ , the field decays, resulting in rapid ringdown to RN-AdS. For slightly larger  $q$ , a growing mode is present, and the instability ensues. We checked that the initial growth rate—while the perturbation remains small—matches the prediction of [10] in the linearized case. At later times, the perturbation becomes nonlinear, as backreaction on the BH becomes significant, with the spacetime eventually settling into a stationary hairy BH.

The superradiant cases display the following characteristics: (i) The scalar field eventually saturates in amplitude and has harmonic time dependence<sup>3</sup>, resulting in a *time-independent* stress-energy tensor and metric; (ii) Significant amounts of charge [measured at the apparent horizon (AH)] are extracted from the BH by the scalar field, with more extracted at larger  $q$ ; (iii) The irreducible mass of the BH (proportional to the square root of the area)<sup>4</sup> approaches that of a Schwarzschild-AdS BH of mass  $M$ , with closer approach for larger  $q$  (implying less mass extraction for larger  $q$ ); (iv) The scalar hair is distributed farther away<sup>5</sup> from the BH for larger  $q$ ; and

(v) The approach to the final state is less smooth for larger  $q$ , in a sense that will be described below.

In Figure 1, we show the irreducible mass and charge of the BH vs. time, for various choices of  $q$ . In the left figure, we compare the irreducible mass  $M_{\text{irr}}$  of the AH of our dynamical BH with that of a (uncharged) Schwarzschild-AdS BH with mass  $M$  (we denote this quantity  $M_0$ ). As expected from the area theorem, the irreducible mass (entropy) never decreases. For small  $q$ ,  $M_{\text{irr}}$  displays very smooth approach to its final value, while for large  $q$ , it displays some step-like behavior prior to reaching a plateau. Moreover, for large  $q$ , the ratio  $M_{\text{irr}}/M_0 \rightarrow 1$ , as depicted in Figure 4.

The right side of Figure 1 shows the charge, both of the AH, and the integrated charge (at each constant time surface and outside the AH) of the scalar field (by charge conservation, these must sum to the ADM charge  $Q$ ). The charge displays much more interesting behavior than the irreducible mass, including some up-and-down oscillations. As with  $M_{\text{irr}}$ , the low- $q$  case is smoothest. We find that for large  $q$ , nearly all of the charge can be extracted from the BH. This contrast between the mass and charge extracted arises because the charge-to-mass ratio of the final state scalar field mode is larger for larger  $q$ .

The less smooth behavior of the instability at large  $q$  can be understood by studying the mode content. In Figure 2 we show a spectrogram of an evolution, where we plot the frequency content of  $\varphi_3(v)$  vs time. This reveals the individual modes present in the solution, and their growth or decay as a function of time. The initial data contain a large number of modes, with real frequencies  $\text{Re}(\omega_n) \approx (2n + 3)/L + C$  in the small BH limit. Most of these do not satisfy the superradiance condition, and they decay rapidly [10]. The lower frequency modes, however, with  $(2n + 3) \lesssim \frac{qQL}{r_H}$ , are unstable, and are visibly growing exponentially in the spectrogram [lower- $\text{Re}(\omega_n)$  modes grow more rapidly]. (In Figure 2 there are eight such modes.) Over time, these modes extract charge and mass from the BH, and one by one (starting at large  $n$ ) they begin to decay, and are re-absorbed by the BH. In the end, the BH is discharged to the level where the fundamental ( $n = 0$ ) mode has zero growth rate, and it remains as the condensate.

The oscillations of Figure 1 can be now understood as an effect of having a mixture of modes, some of which are extracting, and others depositing, charge and mass into the BH. In the end, the BH reaches the hairy state, with all the higher modes having decayed. Similar oscillations for larger- $q$  evolutions were misinterpreted as a “bosenova”, or explosion, in [32]. (The bosenova of [18, 19] arises instead when axion self-interactions cause a collapse of the axion field.) Indeed, for  $q$  just above the instability threshold, there is only a single mode, and evolution displays a very smooth approach to the stationary end state.

Radial profiles of the final state are illustrated in Fig-

<sup>3</sup> Previously constructed hairy black holes [12, 13] have static  $\psi$ . This difference arises because these works make the gauge choice that the Maxwell field vanishes at the horizon, whereas we set it to zero at infinity.

<sup>4</sup> As the stationary stage is reached, the AH location coincides with the event horizon.

<sup>5</sup> This observation highlights the difference between placing an artificial boundary at some location with respect to the BH versus at the boundary of AdS.

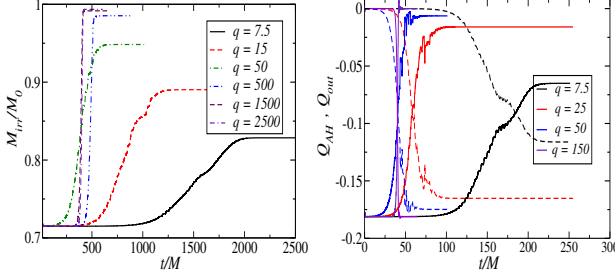


FIG. 1. (Left) (Normalized) Irreducible mass versus time for representative values of  $q$ . As  $q$  is increased the growth rate increases as well. (Right) Charge within the AH (solid), and the charge of the scalar field outside on a constant- $v$  slice (dashed), vs time. As the value of  $q$  is increased, the dynamical time scale shortens. For even smaller  $q$  (not shown), curves are very smooth, with no steps or oscillations. (Note that for the initial data employed, for the largest- $q$  case, most of the scalar field energy falls immediately into the BH as it backscatters off itself, resulting in a smaller effective initial perturbation.)

ure 3. On the left, we plot the Misner-Sharp mass  $M_{\text{MS}}(r)$  (suitably defined so as to take into account the contribution of the AdS curvature [36]) as a function of radius. As  $q$  is increased,  $M_{\text{MS}}$  increases in value at the AH, again confirming that less mass is extracted. As  $\mathcal{I}$  is approached,  $M_{\text{MS}} \rightarrow M$ . Moreover, for large  $q$ ,  $M_{\text{MS}}$  is constant in  $r$  near the BH, while for small  $q$  it grows. This, together with the right figure, shows that the scalar field condensate and the electric field are localized farther away from the BH for larger  $q$ .

Finally, Figure 4 shows the normalized irreducible mass of the final state BH as a function of  $q$ . As  $q$  is increased,  $M_{\text{irr}}/M_0 \rightarrow 1$ . (For  $q = 5000$ ,  $M_{\text{irr}}/M_0 \approx 99.5\%$ .) This, together with the radial profile information, indicates that at late times and large  $q$ , the BH region approaches Schwarzschild-AdS, surrounded by a distant low-mass high-charge condensate.

**Final words.**—We have described the full dynamical behavior of the charged superradiant instability in AdS. Initially, superradiant modes extract charge and mass from the BH and grow exponentially [37]. As this process unfolds, the higher-frequency modes cease to be superradiant, and fall back into the BH, returning energy and charge and resulting in nontrivial dynamics. Eventually, the fundamental mode remains as a condensate, with zero growth. While nonlinear couplings between modes (via gravity and electromagnetism) can generate higher-frequency modes in AdS [16, 17], any such processes are overwhelmed by the fact that in the end, all modes beyond the fundamental are decaying. The ultimate fate is a stable hairy BH, with the scalar condensate distributed far away from the BH for large  $q$ .

Among the scalar modes, the final mode that remains maximizes the charge-to-mass ratio  $q/\omega$ , and its growth corresponds to maximizing the entropy increase of the

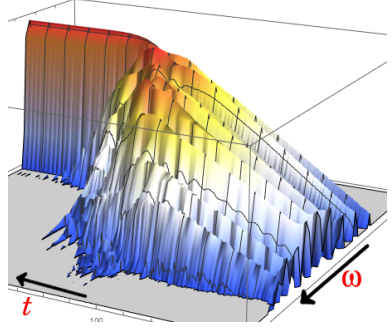


FIG. 2. Spectrogram showing logarithm of amplitude of Fourier transform of  $\varphi_3(v)$  as a function of time. This is computed by partitioning the time axis into intervals of length  $\Delta v = 4\pi$ , and performing discrete Fourier transforms on these intervals. The intervals overlap, with starting points offset by  $\delta v = \pi/8$ . The case here has  $q = 12$ ,  $r_H = 0.2$ , and  $Q$  set to 80% of the extremal value. At early times, the lowest eight modes grow exponentially, with faster growth for lower frequencies. As charge and mass is extracted, all modes (aside from the fundamental) eventually start to decay, with higher frequencies decaying first. The growth rate of the fundamental approaches zero, leaving a final static BH with a harmonically oscillating scalar condensate.

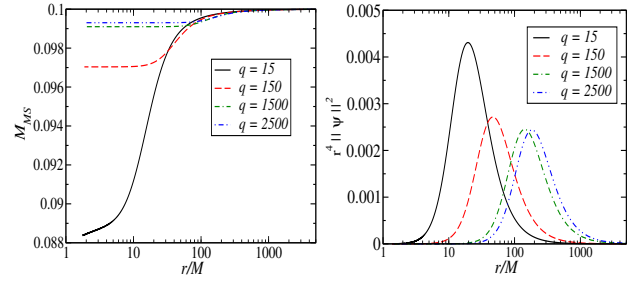


FIG. 3. (Left) Misner-Sharp mass versus radius for representative values of  $q$ , measured for the late-time static spacetime. For large values of  $q$ ,  $M_{\text{MS}}$  is constant to relatively large radial distance, indicating that BH is essentially uncharged and the scalar field hair lies far away from it. At larger radii, a radial dependence arises because of the presence of both the electromagnetic and scalar fields. (Right) Norm (squared and rescaled by  $r^4$ ) of the scalar field, also at late times. The field is localized far from the BH for large values of  $q$ .

BH. This observation may elucidate possible behavior of the superradiant instability in the rotating case. For a Kerr-AdS BH, the stability criterion for a mode is  $\omega < m\Omega_H$ , where  $\Omega_H$  is the angular frequency of the BH, and  $m$  the azimuthal number of the perturbation [4]. This is comparable with the condition  $\omega r_H < qQ$  in the charged case, but with the key difference that  $m$  can take any integer value, whereas  $q$  is a fixed parameter of the system. In the rotating case, a given perturbation may be expected to spin down the black hole to the point where only the most superradiant mode remains (i.e., that which causes the black hole to maximize its entropy), but now just marginally stable. It would be in-

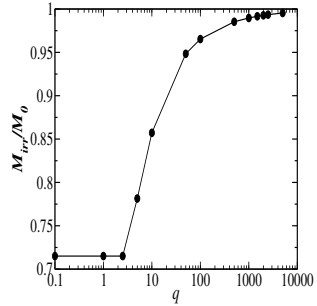


FIG. 4. Normalized irreducible mass vs  $q$ . As  $q$  is increased,  $M_{\text{irr}}/M_0 \rightarrow 1$ . This is consistent with the claim that the final BH state for sufficiently large values of  $q$  is a Schwarzschild-AdS black hole of mass  $M$  (the ADM mass), surrounded by a distant high charge, low-mass scalar field condensate.

teresting to examine the superradiant mode frequencies

in Kerr-AdS presented in [11] from this point of view; it is plausible that the final (i.e., most superradiant) mode has  $m \rightarrow \infty$ , consistent with speculation of [15].

Finally, in astrophysical applications, the outer potential barrier is no longer infinite (as in AdS), and is instead typically provided by a mass term for the field [18, 38, 39]. Such a case provides a cutoff in mode energy, and on the efficiency of energy extraction.

**Acknowledgments.**—We would like to thank A. Buchel, S. L. Liebling, O. Sarbach and J. Winicour for discussions and comments throughout this project. This work was supported in part by NSERC through a Discovery Grant (to L.L.), by CIFAR (to L.L.), by CONACyT-Mexico (to P.B.), and by Perimeter Institute for Theoretical Physics. Research at Perimeter Institute is supported by the Government of Canada through Industry Canada and by the Province of Ontario through the Ministry of Research and Innovation.

## Supplemental Material

### CONTENTS

Numerical method	5
Code validation	7
References	7

### Numerical method

Here we provide additional details of our numerical approach. Our implementation is similar to that of [34], but with several modifications: (1) We include Maxwell and complex scalar fields, (2) Our black hole has spherical (as opposed to planar) topology, (3) We excise the black hole from the computational domain and (4) instead of pseudospectral methods we employ finite differences with derivatives satisfying summation by parts [40, 41].

As noted in the main text, in order to discretize the spacetime, we adopt a compact spatial domain so as to include the AdS boundary ( $\mathcal{I}$ ) in our computational grid and ensure the full equations are consistently implemented. Hence, we introduce  $\rho = 1/r$  as our spatial coordinate and define new variables,

$$A(v, r) = \alpha(v, 1/r) = \alpha(v, \rho), \quad (\text{S1})$$

$$\Sigma(v, r) = \sigma(v, 1/r) = \sigma(v, \rho), \quad (\text{S2})$$

$$d_+ \Sigma(v, r) = s(v, 1/r) = s(v, \rho), \quad (\text{S3})$$

$$W(v, r) = \nu(v, 1/r) = \nu(v, \rho), \quad (\text{S4})$$

$$\psi(v, r) = \varphi(v, 1/r) = \varphi(v, \rho), \quad (\text{S5})$$

$$d_+ \psi(v, r) = \Pi(v, 1/r) = \Pi(v, \rho). \quad (\text{S6})$$

From the asymptotic forms (16)–(19), we see that some of these fields diverge at  $\mathcal{I}$ , so it is more convenient to evolve

$f$	$f _{\rho=0}$	$\partial_\rho f _{\rho=0}$
$\hat{\alpha}$	$-L^2\lambda$	$-2M$
$\hat{\sigma}$	$\frac{1}{2}L^2\lambda$	$0$
$\hat{s}$	$0$	$-M$
$\hat{w}$	$\nu$	$Q$
$\hat{\varphi}$	$0$	$\varphi_3$
$\hat{\Pi}$	$0$	$-\frac{3}{2L^2}\varphi_3$
$\hat{\beta}$	$-2M$	$2L^2\lambda M + \frac{Q^2}{2}$
$\hat{z}$	$Q$	$-L^2\lambda Q$

TABLE I. Boundary conditions for the evolved fields.

“hatted” fields that have better asymptotic behavior. We define

$$\hat{\alpha} = \alpha - \frac{1}{L^2}\sigma^2 - 1, \quad (\text{S7})$$

$$\hat{\sigma} = \sigma - \frac{1}{\rho}, \quad (\text{S8})$$

$$\hat{s} = s - \frac{1}{2L^2}\sigma^2 - \frac{1}{2}, \quad (\text{S9})$$

$$\hat{\nu} = \nu, \quad (\text{S10})$$

$$\hat{\varphi} = \frac{1}{\rho^2}\varphi, \quad (\text{S11})$$

$$\hat{\Pi} = \frac{1}{\rho}\Pi. \quad (\text{S12})$$

In order to integrate a first order system [(10) and (12) have second order space derivatives], we also introduce  $\hat{\beta} = \partial_\rho \hat{\alpha}$  and  $\hat{z} = \partial_\rho \hat{w}$ . With the compact domain, the asymptotic conditions are simply imposed as boundary conditions at  $\rho = 0$  (see Table I).

The equations of motion for the hatted fields are obtained by substitution into the equations already written in the main text. We omit the resulting (lengthy) expressions. Given  $\hat{\varphi}$  at time  $v = v_0$  (more specifically, we keep track of its real and imaginary parts), we integrate eqs. (9), (10), (12), (14), and (15), together with  $\hat{\beta} = \partial_\rho \hat{\alpha}$  and  $\hat{z} = \partial_\rho \hat{w}$ , to obtain all of the remaining hatted fields at time  $v = v_0$ . These equations are all first order in space, so we impose the initial value for each field at  $\rho = 0$ , as listed in the middle column of Table I. To evolve forward in time, we make use of the definition

$$d_+\psi = \partial_v\psi + \frac{1}{2}A\partial_r\psi \quad (\text{S13})$$

(again, re-written in terms of hatted fields), to obtain  $\partial_v\hat{\varphi}$  at time  $v = v_0$ . Knowing this, we evolve forward one step in time, and repeat the procedure.

The boundary conditions in Table I contain two free functions,  $\lambda$  and  $\nu$ , which correspond to the remaining freedom in the choice of radial coordinate and the vector potential after imposing (7) and (8), respectively. We set these quantities to zero, so the only remaining boundary conditions are the (constant) ADM mass and charge ( $Q$  and  $M$ ), which we are free to choose. The final function,  $\varphi_3(v)$ , shown in the table, is not set in advance, but rather is an *output* of the evolution, which may be read off.

The full equations are discretized by adopting a uniform grid  $\rho_i = (i - 1)d\rho$  with  $d\rho = \rho_{\text{inner}}/(N - 1)$  (with  $\rho_{\text{inner}} < \rho_{\text{AH}}$  the location of the AH; see below). Null hypersurfaces are discretized in time separated by  $dv = \gamma d\rho$  with  $\gamma$  chosen typically = 0.4 to ensure satisfying the CFL condition. Radial integrations are performed using a 4th order Runge-Kutta, being mindful of a few subtleties. Some of the equations of motion involve 0/0-type terms at  $\rho = 0$ , in these cases we impose the radial derivative explicitly at the boundary (and where needed regularize the equations via the L'Hôpital rule). (For this reason, we provide the third column of Table I.) Additionally, the equation of motion for  $\hat{s}$  is of the form  $\partial_\rho \hat{s} \sim \hat{s}/\rho + \dots$ , which is problematic as its regularization leaves no equation. We instead use a 2nd order implicit scheme for this equation, making the spatial integration 2nd order as a whole. Time integrations are performed with RK4, and spatial derivatives satisfy the summation by parts property and are 2nd order accurate at boundary points while 4th order accurate at interior ones [40].

As mentioned, we do not exploit the freedom in  $\lambda$  to fix the position of the AH at a constant radial coordinate as in [34]. Rather, we find the AH at each incoming null surface and excising a number of grids points inside of it (typically 10 points; see, e.g., [41, 42]).

### Code validation

We have confirmed the validity of our implementation through extensive tests summarized below:

- By choosing small values of  $q$  and a configuration for the scalar field not satisfying the superradiance condition we have confirmed the decay of the perturbations and with a rate in agreement with those presented in [10]. Our extracted values for both real and imaginary parts of  $\omega$  agrees with those obtained in linearized perturbations to better than 0.01% even with relatively modest resolutions ( $N = 801$ ).
- Choosing instead larger values of  $q$  we obtained the onset of the superradiance instability and confirmed our extracted values agree with those in [10] with high accuracy.
- An even more stringent test is provided by evaluating independent residuals—furnished by the equations (11) and (13). That is, we independently evaluate these equations, discretized in a straightforward second order approximation, employing fields at two sequential time slices, and confirmed the equations are satisfied to this order throughout our evolutions.
- All results presented here have been validated by employing several distinct resolutions. Typical resolutions of  $N = 1601$  points suffice for excellent accuracy for low to mid values of  $q$  while we adopt higher ones  $N = 3201$  or  $N = 4801$  for  $q > 1000$ .
- We performed self-convergence tests showing that our numerical solutions converge at least to second order.

---

\* pbosch@perimeterinstitute.ca

† sgreen@perimeterinstitute.ca

‡ llehner@perimeterinstitute.ca

- [1] Y. B. Zel'dovich, Soviet Physics-JETP **35**, 1085 (1972).
- [2] A. A. Starobinskij, Zhurnal Eksperimentalnoi i Teoreticheskoi Fiziki **64**, 48 (1973).
- [3] W. H. Press and S. A. Teukolsky, Nature **238**, 211 (1972).
- [4] S. Hawking and H. Reall, Phys. Rev. **D61**, 024014 (1999), arXiv:hep-th/9908109 [hep-th].
- [5] V. Cardoso and O. J. Dias, Phys. Rev. **D70**, 084011 (2004), arXiv:hep-th/0405006 [hep-th].
- [6] S. R. Green, S. Hollands, A. Ishibashi, and R. M. Wald, (2015), arXiv:1512.02644 [gr-qc].
- [7] D. Christodoulou and R. Ruffini, Phys. Rev. **D4**, 3552 (1971).
- [8] G. Denardo and R. Ruffini, Phys. Lett. B **45**, 259 (1973).
- [9] J. D. Bekenstein, Phys. Rev. **D7**, 949 (1973).
- [10] N. Uchikata and S. Yoshida, Phys. Rev. D **83**, 064020 (2011), arXiv:1109.6737 [gr-qc].
- [11] V. Cardoso, O. J. C. Dias, G. S. Hartnett, L. Lehner, and J. E. Santos, JHEP **04**, 183 (2014), arXiv:1312.5323 [hep-th].
- [12] P. Basu, J. Bhattacharya, S. Bhattacharyya, R. Loganayagam, S. Minwalla, and V. Umesh, JHEP **10**, 045 (2010), arXiv:1003.3232 [hep-th].
- [13] O. J. C. Dias, P. Figueras, S. Minwalla, P. Mitra, R. Monteiro, and J. E. Santos, JHEP **08**, 117 (2012), arXiv:1112.4447 [hep-th].
- [14] O. J. C. Dias, J. E. Santos, and B. Way, JHEP **12**, 171 (2015), arXiv:1505.04793 [hep-th].
- [15] B. E. Niehoff, J. E. Santos, and B. Way, (2015), arXiv:1510.00709 [hep-th].
- [16] P. Bizon and A. Rostworowski, Phys. Rev. Lett. **107**, 031102 (2011), arXiv:1104.3702 [gr-qc].
- [17] V. Balasubramanian, A. Buchel, S. R. Green, L. Lehner, and S. L. Liebling, Phys. Rev. Lett. **113**, 071601 (2014), arXiv:1403.6471 [hep-th].
- [18] A. Arvanitaki and S. Dubovsky, Phys. Rev. D **83**, 044026 (2011), arXiv:1004.3558 [hep-th].
- [19] H. Yoshino and H. Kodama, Prog. Theor. Phys. **128**, 153 (2012), arXiv:1203.5070 [gr-qc].
- [20] P. Pani, V. Cardoso, L. Gualtieri, E. Berti, and A. Ishibashi, Physical Review Letters **109**, 131102 (2012), arXiv:1209.0465 [gr-qc].
- [21] J. M. Maldacena, Int. J. Theor. Phys. **38**, 1113 (1999), [Adv. Theor. Math. Phys. 2, 231 (1998)], arXiv:hep-th/9711200 [hep-th].
- [22] M. Guica, T. Hartman, W. Song, and A. Strominger, Phys. Rev. **D80**, 124008 (2009), arXiv:0809.4266 [hep-th].

- [23] O. J. C. Dias, R. Emparan, and A. Maccarrone, Phys. Rev. **D77**, 064018 (2008), arXiv:0712.0791 [hep-th].
- [24] K. Murata, Prog. Theor. Phys. **121**, 1099 (2009), arXiv:0812.0718 [hep-th].
- [25] I. Bredberg, T. Hartman, W. Song, and A. Strominger, JHEP **04**, 019 (2010), arXiv:0907.3477 [hep-th].
- [26] G. Compere, Living Rev. Rel. **15**, 11 (2012), arXiv:1203.3561 [hep-th].
- [27] M. Dafermos and I. Rodnianski, (2010), arXiv:1010.5132 [gr-qc].
- [28] M. Dafermos, I. Rodnianski, and Y. Shlapentokh-Rothman, (2014), arXiv:1402.7034 [gr-qc].
- [29] L. Lehner, Class. Quant. Grav. **18**, R25 (2001), arXiv:gr-qc/0106072 [gr-qc].
- [30] M. W. Choptuik, L. Lehner, and F. Pretorius, ArXiv e-prints (2015), arXiv:1502.06853 [gr-qc].
- [31] W. E. East, F. M. Ramazanoğlu, and F. Pretorius, Phys. Rev. D **89**, 061503 (2014), arXiv:1312.4529 [gr-qc].
- [32] N. Sanchis-Gual, J. C. Degollado, P. J. Montero, J. A. Font, and C. Herdeiro, (2015), arXiv:1512.05358 [gr-qc].
- [33] S. S. Gubser, Phys. Rev. **D78**, 065034 (2008), arXiv:0801.2977 [hep-th].
- [34] P. M. Chesler and L. G. Yaffe, JHEP **07**, 086 (2014), arXiv:1309.1439 [hep-th].
- [35] K. Murata, S. Kinoshita, and N. Tanahashi, JHEP **07**, 050 (2010), arXiv:1005.0633 [hep-th].
- [36] H. Maeda, Phys. Rev. **D86**, 044016 (2012), arXiv:1204.4472 [gr-qc].
- [37] R. Brito, V. Cardoso, and P. Pani, eds., *Lecture Notes in Physics, Berlin Springer Verlag*, Lecture Notes in Physics, Berlin Springer Verlag, Vol. 906 (2015) arXiv:1501.06570 [gr-qc].
- [38] T. Damour, N. Deruelle, and R. Ruffini, Lett. Nuovo Cim. **15**, 257 (1976).
- [39] S. L. Detweiler, Phys. Rev. **D22**, 2323 (1980).
- [40] G. Calabrese, L. Lehner, D. Neilsen, J. Pullin, O. Reula, O. Sarbach, and M. Tiglio, Class. Quant. Grav. **20**, L245 (2003), arXiv:gr-qc/0302072 [gr-qc].
- [41] A. Buchel, L. Lehner, and R. C. Myers, JHEP **08**, 049 (2012), arXiv:1206.6785 [hep-th].
- [42] R. Gomez, L. Lehner, R. L. Marsa, and J. Winicour, Phys. Rev. **D57**, 4778 (1998), arXiv:gr-qc/9710138 [gr-qc].